The final stages of capillary break-up of polymer solutions

R. Sattler, S. Gier, J. Eggers, and C. Wagner

Citation: Phys. Fluids **24**, 023101 (2012); doi: 10.1063/1.3684750
View online: http://dx.doi.org/10.1063/1.3684750
View Table of Contents: http://pof.aip.org/resource/1/PHFLE6/v24/i2
Published by the American Institute of Physics.

The final stages of capillary break-up of polymer solutions

R. Sattler,[1] S. Gier,[1] J. Eggers,[2] and C. Wagner[1,a)]
[1]*Experimentalphysik, Universität des Saarlandes, Postfach 151150, 66041 Saarbrücken, Germany*
[2]*School of Mathematics, University of Bristol, University Walk, Bristol BS8 1TW, United Kingdom*

(Received 29 September 2011; accepted 19 January 2012; published online 14 February 2012)

The capillary break-up of a polymer solution evolves via a series of stages. After the initial instability a long-lived cylindrical filament is formed, which thins exponentially in time, while the flow is purely extensional. During the final stages of the thinning process, at which the polymers are stretched sufficiently for the filament to become unstable to a Rayleigh–Plateau-like instability, a complex flow pattern develops, which we describe here. Achieving a high spatial resolution well below the optical Rayleigh limit, we describe both the formation of individual droplets as well as that of periodic patterns. Following the periodic instability, a blistering pattern appears, with different generations of smaller droplets. At sufficiently high polymer concentrations, the filament does not break at all, but a solid polymeric fiber with a thickness well below a micron remains. The experiments were performed for various polymer and solvent systems, all of which showed the same qualitative behavior for most of the observed features. © *2012 American Institute of Physics*. [http://dx.doi.org/10.1063/1.3684750]

I. INTRODUCTION

When a droplet of a simple liquid is placed between two plates which are drawn apart gently, the liquid bridge becomes unstable to the Rayleigh–Plateau instability. The final stages of pinch-off are governed by self-similar laws,[1,2] and the minimum neck diameter decreases linearly in time, at least if viscous forces dominate inertial ones. An alternative experiment is that of a droplet detaching from a faucet. As the pinch-off phenomena reported here are local in character, both experiments yield similar results.

The addition of a small amount of flexible high molecular weight polymer does not alter the primary Rayleigh–Plateau instability significantly. But when the flow becomes strong enough,[3] the polymer chains are stretched, and the effective viscosity of the solution increases dramatically, slowing down the pinching.[4] The experiment using a polymeric liquid can be repeated by the reader quite easily, by placing a droplet of saliva between two fingers and separating them (see Fig. 1). One observes the formation of a cylindrical filament, while the bulk of the fluid collects in two "main" droplets at the upper and lower end. The reason for the formation of the filament is that any localized pinching produces a corresponding extensional flow, by which polymers are stretched. Thus the viscosity increases, and further pinching is inhibited.

The flow inside the filament is purely extensional, and polymers are stretched continuously, resulting in a strong increase of the viscosity. This leads to thinning of the filament according to an exponential law,[4–11] as opposed to the finite time singularity found for a Newtonian liquid.[2] At the end of stretching process, the polymer solution possesses an elongational viscosity several orders of magnitude greater than that of the solvent. The polymers in the main drop remain in an essentially relaxed state. Both the experimental and the theoretical determination of the elongational viscosity of complex liquids remain a challenging task, and capillary break-up experiments are a common

a)Electronic mail: c.wagner@mx.uni-saarland.de.

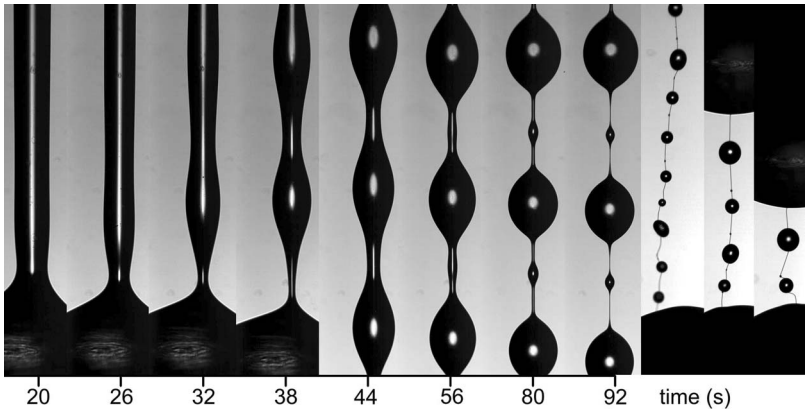

FIG. 1. The final stages of the break-up of a droplet of human saliva (for $t \leq 92$ s images are 0.21×1.37 mm, the last three images are 0.42×3.1 mm). Its behavior is representative of other model polymer solutions described here, but note the slow time scale, which is in the order of a minute. Time is counted from the formation of a cylindrical filament, which is shown in the first panel. The filament is bordered by a large "main" bead at the bottom, only a small part of which is shown, to accommodate a sufficient number of images. At $t = 26$ s a constriction forms above the lower drop, and a small bead becomes visible just above it. From about $t = 38$ s, the filament is unstable to the formation of a periodic array of droplets, akin to a Rayleigh instability. Subsequently, a blistering pattern of droplets of very different sizes is formed. The filament remained stable for several minutes, and final rupture was initiated by agitating the system. This is shown in the magnified last three images on the right. They illustrate the stiffness of the (solid) polymeric fiber that is formed between the remaining droplets and which remains essentially straight.

method of deducing extensional rheological properties of a liquid sample. A commercial version of this capillary break-up rheometer is also available (CaBER, Thermo Fisher Scientific, Karlsruhe, Germany).

A highly stretched filament is shown in the first panel of Fig. 1, near the lower main drop. In the next two panels, an isolated droplet grows at the lower end of the filament, followed by the formation of a periodic structure. Since any localized pinching is stabilized by a further increase of the polymeric viscosity, we conclude that the instability of the cylindrical filament is associated with the polymer strands having reached nearly full stretch. We will refer to all structures resulting from the instability of a highly stretched polymer strand as a "blistering" pattern. From the 5th to the 8th panel, the periodic structure becomes increasingly nonlinear, leading to the formation of smaller drops of widely varying sizes.[12,13] Eventually a solid nano fiber is formed as a long-lasting remnant of the fluid filament,[14] shown in the last three panels of Fig. 1. As illustrated in Fig. 1, only strong mechanical perturbations can break the fiber.

There exist two fundamentally different physical mechanisms leading to the formation of drops (or beads) of different sizes on a polymeric filament. The first is associated with the "beads-on-a-string" structure,[3,5–8,11] and refers to the formation of a drop pattern out of an initially relaxed state. Essentially, this pattern is closely related to the drop and satellite drop structure produced by the Newtonian solvent alone. Inside a drop the polymer remains relaxed, but in the fluid necks in between the polymer becomes stretched, leading to the formation of cylindrical filaments. The result is a pattern which alternates between almost spherical drops and thin filaments, which thin at an exponential rate.[6,10]

If the solvent viscosity is small, the beads-on-a-string mechanism can lead to more complicated patterns including smaller satellite drops between main drops,[15] which are a remnant of the corresponding structure observed for Newtonian liquids. This correspondence was analyzed experimentally and theoretically in Ref. 3, where it was shown that the formation of satellites depends on the relation between the polymer timescale and the timescale of the initial inviscid Rayleigh instability. More detailed experimental[16] and computational[17,18] studies have investigated the conditions under which more complicated beads-on-a-string structures may be formed. Note that from a point of view of theoretical modeling, the beads-on-a-string structures should be well described by the Oldroyd-B model, which allows for unlimited stretch of polymers. As a result, polymeric filaments will never break in this description, but continue to thin exponentially.

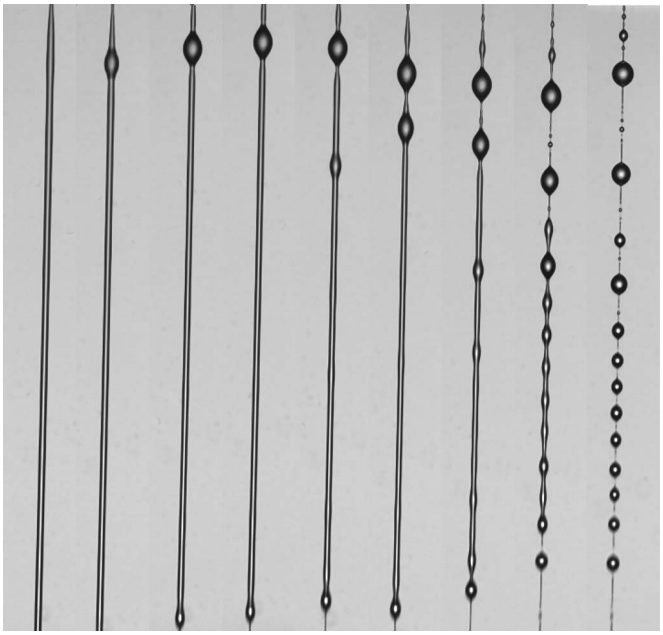

FIG. 2. The final stages of the breakup of a droplet of 2000 ppm PEO in 60/40 wt% glycerol/water. Images are 0.11 × 0.93 mm, and the time interval between images varies between 5 and 20 ms. The solvent viscosity is about 10 times that of water. One observes the growth of isolated beads at the bottom and at the upper end, as the growth of a coherent pattern.

The blistering mechanism investigated here, by contrast, starts from a highly stretched filament, and proceeds to a structure of partially relaxed states, composed of very small droplets, joined by filaments. As explained above, this instability is related to polymer strands reaching full stretch, and can only be described theoretically with models which include the finite extensibility of polymers, such as the Giesekus or FENE models.[19] In Ref. 20, it was shown that finite extensibility leads to a transition from exponential to localized linear thinning, as expected for a Newtonian fluid. The solvent viscosity, on the other hand, is unimportant, as illustrated in Fig. 2, using a solvent 10 times more viscous than the pure water used elsewhere in this study. Yet essentially the same phenomena of isolated and coherent bead growth are observed. This is to be expected, since the extensional viscosity of polymer solution is far greater than that of the solvent.

In Ref. 21, the formation of a hierarchy of thinner and thinner filaments out of an initial, highly stretched polymeric filament was predicted on the basis of a sequence of instabilities. The mechanism for the instability, however, remained unclear since the calculation was performed in the framework of the Oldroyd-B model, for which a filament should be stable.[10,20] The formation of a hierarchy of beads and connecting filaments from a highly stretched polymeric fiber was investigated experimentally in Refs. 12 and 13. The process was found to be self-similar, but the scaling laws were different from those predicted by Ref. 21.

The current paper is an extension of an earlier study.[14] We focus on the blistering instabilities suffered by the thin filament containing a solution of highly stretched polymers. We find that the sequence of instabilities suffered by the polymeric filament is considerably more complicated than reported earlier, and consists of both localized and period patterns. We try to gain insight into the physical properties of each type of instability investigated. At the end a solid fiber is formed,[14] whose properties and instabilities we investigate in detail.

II. EXPERIMENTAL SETUP AND SAMPLE SOLUTIONS

A. Experimental setup

Capillary break-up was studied using both the CaBER setup and drops falling from a faucet. For the former a well defined quantity of the sample liquid is placed with a pipette between two

steel discs with a diameter of 2 mm. The lower disc is fixed and the upper disc can be drawn apart with a linear motor (P01-23x80, Linmot, Spreitenbach, Switzerland). For the latter, the liquid was driven quasi-statically with a syringe pump through a nozzle of a diameter of 3 mm. Both protocols lead to very similar results, but with the CaBER setup it was easier to obtain high optical resolution data while with the droplet experiment it was easier to obtain good statistics as the nozzle could be feed continuously and one could observe many droplets in a row.

A 100 W halogen lamp with an infrared shield is used to produce a shadowgraph image of the capillary bridge. The cylindrical filament is optically almost identical to a cylinder lens. Light that passes through the center of the filament is not diffracted and produces a bright line in the middle of the filament (cf. Fig. 1). Light that passes through the outer regions is diffracted, so these parts of the filament appear dark. The filament is filmed by a 10bit high speed camera (X-Stream XS-5, IDT, Tallahassee, USA) at 1 kHz frame rate and 1 ms shutter time. The camera has 1280x1024 pixels with a size of 12×12 μm. Microscope objectives with different magnifications of 4, 10, and 20 fold were used. The latter is a Nikon long working distance objective ($WD = 7$ mm) with a numerical aperture of $NA = 0.45$. At the shortest light wave length with reasonable sensitivity of the camera of $\Lambda \approx 450$ nm, this yields a diffraction limited resolution of δ=0.6 μm.

To observe the growth of very small perturbations on the polymeric filament, the resolution has to be improved far below this value. In Ref. 14, we showed that we could resolve the amplitude of the sinusoidal deformation of the cylindrical filament down to a resolution of 80 nm. This was achieved by fitting the data to a model profile of a sine function with wave number, phase, and amplitude as free parameters over many wavelengths. This method that is often referred to as super-resolution is thus nonlocal in character. To be able to observe localized objects with an equally high resolution, we have developed a completely different technique, which is based on intensity data along a cut perpendicular to the filament axis alone, see Fig. 3. The details will be published in a separate publication.[22]

The idea is to calculate the light intensity near the edge of a long and perfectly absorbing object of a given thickness, using Fresnel theory. We then model our light source as a black body of temperature $T = 3000$ K and perform the convolution of the diffraction pattern for a given wave length with the energy density distribution of a black body. As a result, most of the oscillations presented in the Fresnel diffraction pattern go away and only a single maximum remains, see Fig. 3. The resulting theoretical curve can be fitted to the experimental grey scale data, using the filament thickness as an adjustable parameter. Using this technique, we were able to bring down the achievable spatial resolution to a precision of 30 nm. The accuracy of this method is not as good and could be estimated to 1 μm. We are mostly interested in relative deformations of our filament and then the reproducibility is the more relevant quantity.

The depth of field of our optical setup was 5 μm, which made it very difficult to obtain sharp images at the last stages. Filaments with a thickness of $d \approx 10$ μm near the end of the thinning

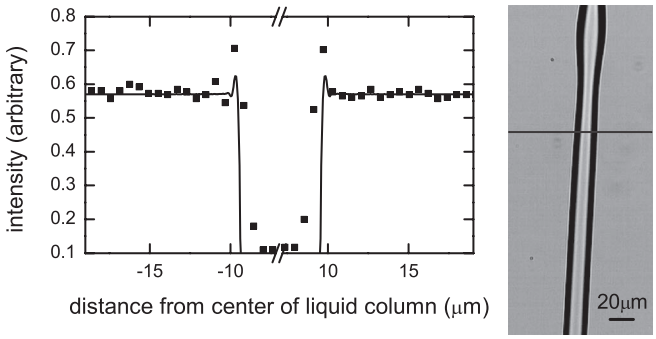

FIG. 3. Right: Grey level image of a viscoelastic filament. The black line indicates the position where the intensity distribution for the left graph was determined. Left: Measured (square symbols) and simulated (black line) intensity distribution around the viscoelastic filament. The theoretical data are obtained by calculating the Fresnel diffraction from an object of thickness 19μm, and convolving it with the energy distribution of black body radiation.

TABLE I. Samples used in this study.

Abbreviation	Polymer	Solvent	c_p(ppm)	η_s(mPas)	$p_{v,25^\circ C}$(kPa)
PEO_{1k-w}	Poly(ethylene oxide)	Water	1000	1	3.17
PEO_{2k-w}	Poly(ethylene oxide)	Water	2000	1	3.17
PEO_{2k-x}	Poly(ethylene oxide)	Xylol	2000	0.61	1.11
PEO_{2k-gl}	Poly(ethylene oxide)	40 wt% water + 60 wt% glycerol	2000	0.59	10.7
$PAAA_{2k-ws}$	Poly(acrylamide-co-acrylic acid)	Water + 10 wt% sugar	2000	1.17	2.85
PS_{2k-dep}	Polystyrene	Diethylphthalate	2000	8.75	0.00022
PS_{2k-dmf}	Polystyrene	Dimethylformamide	2000	0.796	0.493

process were very sensitive to slightest distortions by air currents or showed non-reproducible lateral movements in the order of several microns even when air currents were mostly suppressed by an additional glass box around the capillary bridge. Only one in a hundred tries yielded images that were sharp enough to allow a quantitative analysis with the sub-diffraction limited resolution discussed above.

Still, all other measurements could be used, e.g., to determine the distribution of the final sizes of the secondary droplets. The study of the very final stages was possible with the CaBER setup only and by performing a protocol that differs from that of other groups,[23] who try to pull the discs apart as quickly as possible. However, this introduces additional oscillations on the capillary bridge, which are prohibitively large for the observation of the final nano fiber regime. Instead, we used a protocol described in Ref. 24, in which the two plates were moved apart slowly up to a distance of $l = 2.5$ mm first, then held for several seconds to allow the liquid to fully relax. Then the plates were drawn to $l = 3.5$ mm within 40 ms, only slightly exceeding the elongation necessary to initiate the Rayleigh–Plateau instability leading to break-up. The release of capillary tension in the two remaining half drops at both ends of the capillary bridge also lead to oscillations, but they were sufficiently small to have vanished by the time the nano fiber was formed.

B. The sample solutions

Most of our quantitative measurements were performed with polyethylenoxide (PEO, $M_w = 4 \times 10^6$ g/mol) solutions in water, which is a model system for studies of capillary break-up of polymer solutions. PEO is a very flexible polymer that is available at high molecular weights. To test the general validity of our findings, especially of the final phase separation process and the formation of the solid polymeric nano fiber, a series of measurements on very different polymer and solvent systems have also been performed. In choosing other systems, we varied the solvent viscosity η_s, as well as the polarity and the vapor pressure p_v of the solvent (see Table I). These other systems were 2000 ppm PEO ($M_w = 4 \times 10^6$ g/mol) in Xylol, 2000 ppm polystyrene ($M_w = 8 \times 10^6$ g/mol) in diethylphthalate and in dimethylformamide, 2000 ppm poly(acrylamide-co-acrylic acid) (PAAA, $M_w = 5 \times 10^6$ g/mol) in a 10 wt% sugar water solution and human saliva, which has been obtained from a healthy donor.

The PEO solutions were characterized by steady shear rheology. The PEO_{2k-w} is shear thinning in the range $0, 1 < \dot{\gamma} < 2000\,s^{-1}$. The zero shear viscosity is $\eta_0 \approx 50$ mPas, and the stationary value at high shear rates $\eta_\infty \approx 4$ mPas.[10,12,25,26] The surface tension as determined by the pendant drop method is $\gamma \sim 60.9$ mN/m. The characteristic time constant evaluated from the exponential thinning regime was very sensitive to aging. For example, the time constant of the PEO sample decreased from 130 ms to 40 ms after four days.

III. OVERVIEW

The main stages of the evolution of a polymeric filament are illustrated in Fig. 4. The filament has formed from a relaxed state owing to the stretching of polymers by the extensional flow inside the filament. The flow is driven by the capillary pressure difference between the thin thread and the

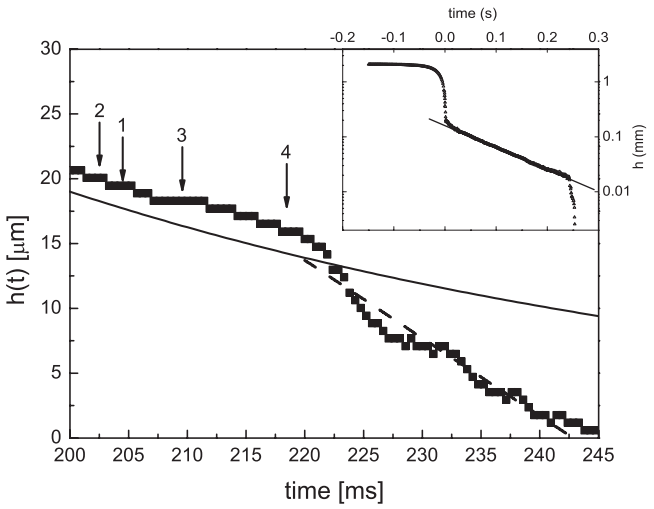

FIG. 4. Inset: The minimum radius $h_{\min}(t)$. First the primary Rayleigh–Plateau instability evolves until at $t = 0$ ms the polymers arrest the flow and a cylindrical filament is formed. The full line is an exponential fit to $h_{\min}(t)$ with time constant $\tau \equiv \dot{\epsilon} = 130 \pm 30$ ms. This study focuses on the final stages only which is shown in the main graph. The full line is the same exponential fit as in the inset. From $t = 200$ ms, the filament becomes unstable to first a "breathing instability" and then to the growth of droplets. The arrows indicate the times corresponding to the growth of droplets of the types shown in Fig. 5. We observed single drops at the upper end (1), at the lower end (2) and in between along the filament (3), and the periodic structure (4). At later stages, the time dependence of $h_{\min}(t)$ turns from exponential to linear (dashed line), with slope $\alpha \approx 6 \times 10^4$ m/s.

neighboring drops, which are at a much lower pressure. The pressure inside the thread is $p = \gamma / h_{\min}$, where γ is the surface tension and $h_{\min}$ the thread radius, which is very nearly constant during the initial stages of thinning. The capillary pressure $2\gamma/R$ (R being the drop radius) inside the drop is negligible by comparison. As a result, the fluid contained in the filament is emptying into the drops, producing an elongational flow with elongation rate,

$$\dot{\epsilon} = \frac{\partial_t h_{\min}}{h_{\min}}. \tag{1}$$

On one hand, polymers are being stretched by the flow at a rate $\dot{\epsilon}$, leading to exponential increase in the stress,

$$\sigma_{zz} = \sigma_0 e^{\dot{\epsilon} t}, \tag{2}$$

supported by the polymers. Throughout, we will be concerned with solvents of low viscosity, whose contribution to the total stress is negligible except at the very first stages of break-up, not considered here. On the other hand, the stress (2) is being balanced by the capillary pressure difference, which implies that the drop radius has to decrease like

$$h = h_0 e^{-\dot{\epsilon} t}, \tag{3}$$

consistent with a constant $\dot{\epsilon}$, defined by Eq. (1).

The value of $\dot{\epsilon}$ is set by the balance between stretching and polymer relaxation, which leads to Ref. 6 $\dot{\epsilon} = 1/(3\lambda_p)$, where λ_p is the polymer relaxation time. Typical values for our experiment are $\lambda_p \approx 50$ ms. The growth of polymeric stress is often reported in terms of the *extensional viscosity* $\eta_E \equiv \sigma_{zz}/\dot{\epsilon}$. To compute η_E, the flow in the crossover region between the thread and the drop has to be evaluated,[10] giving

$$\eta_E \equiv \frac{\sigma_{zz}}{\dot{\epsilon}} = \frac{3\lambda_p \gamma}{h_{\min}(t)}. \tag{4}$$

For the case of our model system PEO_{2k-w} (see Table I), the extensional viscosity reaches $\eta_E \approx 300$ Pas at $t = 0.2$ s, counted from the formation of the filament. This is five orders of magnitude

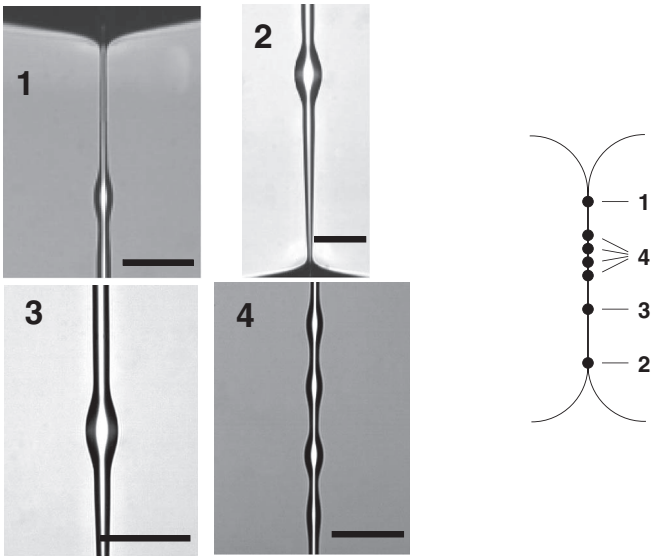

FIG. 5. We observed four different kinds of instabilities leading to the formation of small droplets, which comprise the "blistering" phenomenon. On the left, we sketch the location at which they appear, on the right the droplet formation is shown on a thinning filament of PEO_{2k-w} solution. Single growing droplets are distinguished according to their axial position on the filament: at the upper end (1), at the lower end (2), and in the middle (3) of the thread. The fourth type is a sequence of beads growing coherently (4). The black bar indicates a length of $100\,\mu$.

larger then the elongational viscosity of the solvent, given by $\eta_E(\text{water}) = 3\eta_{\text{shear}} = 3\,\text{mPas}$. As long as the polymers continue to stretch, the filament is very stable: any local acceleration of its thinning rate leads to greater stretch. But increased stretch enhances the polymer stress, inhibiting further pinching. This observation explains the uniformity of the filament. However, at $t = 200\,\text{ms}$ in Fig. 4, the polymers become fully stretched and the filament becomes unstable to a variety of instabilities.[14,20] Based on this idea, Fontelos and Li.[20] have argued that the dynamics of these instabilities proceeds as if the fluid possessed an effective Newtonian viscosity $\eta_{eff} \approx \eta_E$. At this time, the thinning also ceases to be exponential.

The first instability that is usually observed in low viscosity solvents has been described in Ref. 14 as "breathing", which consists of periodic constrictions of the end of the filament. During a constriction, the flow into the end drop is blocked, and as a result the extensional flow in the thread stops. This is seen most clearly in the motion of tracer particles inside the thread, illustrating very nicely the coupling between the interior of the thread and the crossover region toward the drop. During the phase in which the flow stops, the thread ceases to thin, which is seen as small plateaus in the minimum radius, plotted a function of time in Fig. 4.

Next we observe a variety of instabilities leading to the formation of tiny beads, illustrated in Fig. 5. In earlier work of us and others,[12–14] the focus was on instabilities leading to the growth of periodic arrays of droplets, denoted by Eq. (4) below. As expected for a linear instability, the shape of the sequence of beads is sinusoidal, and the amplitude grows exponentially. We termed this phenomenon "blistering",[14] to emphasize the fact that it results from the partial relaxation of polymer stress from a highly extended state, during the last stages of pinching. The well-known "beads-on-a-string" structure,[10] by contrast, originates from a relaxed state in the earliest stages of pinching, leading to a periodically stretched and relaxed state.

In the present paper, we observe that apart from type (4) periodic beads there are three more distinct types of instabilities, leading to the formation of isolated droplets. The isolated droplets are well fitted by a Gaussian profile. For simplicity, we will refer to all instabilities, born out of a highly stretched state, as "blistering". Droplets can appear at the upper end of the thread (1), the lower end of the thread (2), or in the middle of the thread (3), see Fig. 5. All beads grow exponentially at first, once more indicating a linear instability. The beads at the lower end of the thread (2) and in

the middle of the thread (3) then continue to grow like a power law, a fact we will explain below. The growth of all types of beads eventually saturates and the bead size reaches a plateau. Note that gravitational draining appears to be important, in that the instability observed at the upper end of the filament is different from that observed at the lower end. Figure 4 shows a detail of the minimum radius, illustrating the sequence of events in a particular case.

After the beads have reached their final, constant size, a second nonlinear phase is observed, during which beads interact. This leads to the creation of successively smaller beads, which has some aspects of self-similarity. We will refer to them as successive generations of beads. Ultimately, one would expect the filament between two beads to thin further and break. However, it is usually observed that the filament does not break at all, but persists permanently. Instead, a solid nano fiber is formed, which will be described in Sec. VI.

IV. THE LINEAR INSTABILITY

All data presented in this section were taken on the PEO_{2k-w} solution in a CaBER experiment. We found that once the cylindrical filament was sufficiently stretched, it became unstable to four different types of surface distortions, illustrated in Fig. 5. In the following, we will characterize the amplitude-time law of the different types of beads. The timing of the measurements is illustrated in Fig. 4. The profile of the deformed filament was fitted either with a Gaussian for single beads or a sine function for the coherent forms.

A. Isolated beads

The form of the isolated droplets is well approximated by

$$h(z,t) = h_0(t) + \frac{a(t)}{w(t)\sqrt{\pi/2}} e^{-2\left(\frac{z-z_c(t)}{w(t)}\right)^2}, \tag{5}$$

see Fig. 6. Here $h_0(t)$ is the radius of the filament outside the drops and $a(t)$, $w(t)$, and $z_c(t)$ are the amplitude, width, and position of the perturbation.

Droplets at the lower end and in the middle of the filament (type (2) and (3)), grow on conical portions of the filament, whose conical shape is essentially undisturbed, apart from the outward bulge of the drop. By contrast, droplets near the upper liquid reservoir (type (1), see Fig. 5), exhibit an inward bulge at their lower end, which interrupts the conical shape of the filament. Droplets of type (1) grow in parallel to the "breathing" instability at the edge of the filament, described in more

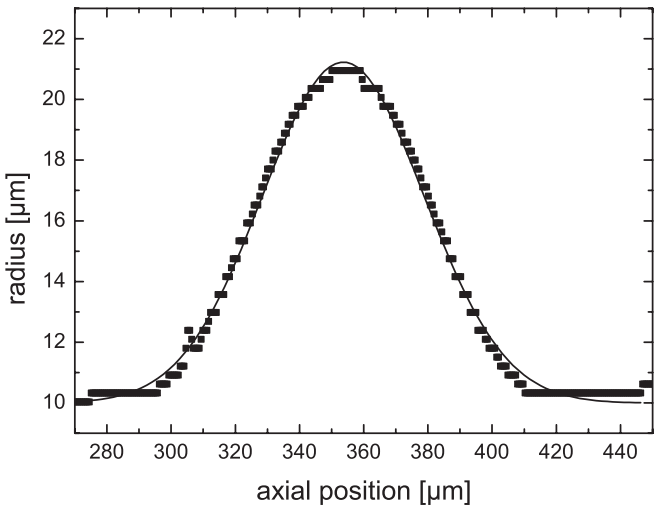

FIG. 6. Radial profile of the single drop (3) shown in Fig. 5 with a Gaussian fit according to Eq. (5).

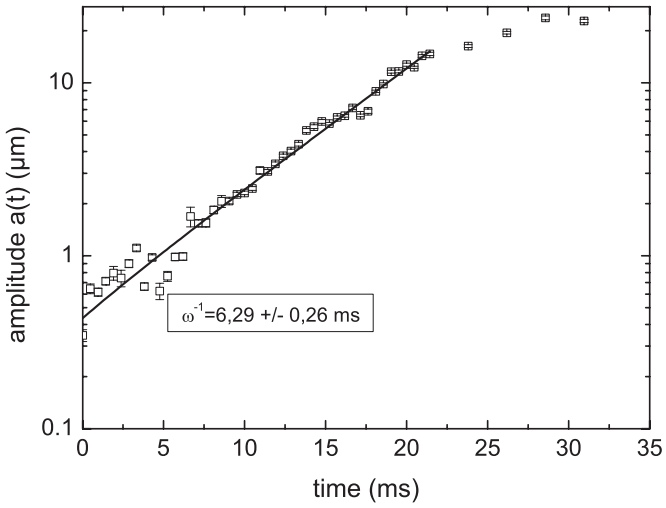

FIG. 7. Temporal evolution of the amplitude of beads of type (1), which appear at the upper end of the filament (see Fig. 5). Experimental data from four different runs agree well with the exponential growth law (6).

detail in Ref. 14. Their amplitude increases exponentially over a period of 15–20 ms, obeying the functional form

$$a_e(t) = a_0 + a_1 \exp(\omega t), \tag{6}$$

shown in Fig. 7. After the time of exponential growth the radius remains constant, and the drops remains at constant volume. The growth rate ω obtained from the fit is reported in Table II. There is no theory that describes the Rayleigh–Plateau instability on a highly stretched viscoelastic filament, but the linear stability of a viscous fluid thread of effective viscosity η_{eff}[2] predicts

$$\omega = \frac{\gamma}{6h_0\eta_{eff}}, \tag{7}$$

TABLE II. The inverse rate of growth ω^{-1}, the filament radius $h_{\min}$ at the beginning of the growth of the respective droplets and the effective elongational viscosity η_{eff} calculated according to Eq. (7) for the different types of beads (indicated by numbers in brackets). Below, the elongational viscosity as estimated from the exponential thinning of $h_{\min}$, cf. Eq. (4), and according to the linear law (9). The values for the growing beads refer to all our measurements with resolution good enough to allow for quantitative analysis.

Type	ω^{-1} [ms]	$h_{\min}$ [μ m]	η_{eff} [Pas]
(1)	6.3	8.6	7.6
(1)	9.8	8.6	11.6
(1)	6.9	8.6	8.4
(1)	6.9	8.0	9.0
(2)	1.6	11.5	1.4
(3)	1.1	10.3	1.1
(3)	1.2	9.2	1.3
(4)	3.6	7.0	5.3
(4)	1.9	7.0	2.8
(4)	2.1	8.6	2.5
(4)	4.2	8.6	5.1
(4)	3.1	8.0	4.0
(4)	9.0	12.0	9.0
Eqs.			
(4)			300 ± 15
(9)			8 ± 2

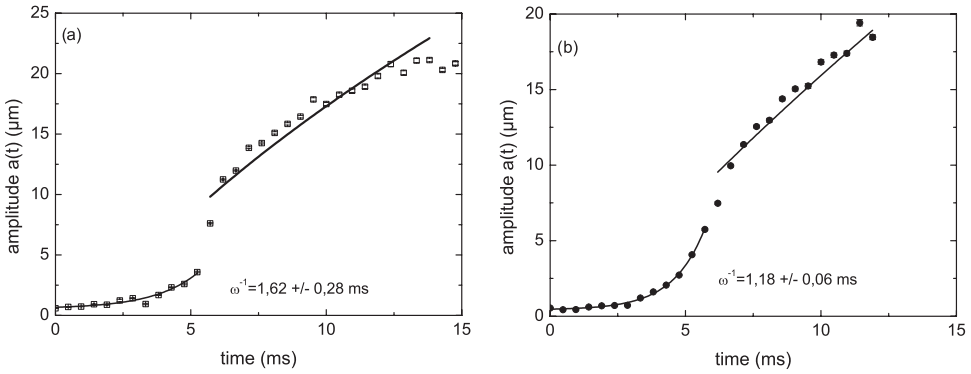

FIG. 8. (a) Temporal evolution of the amplitude of beads of type (2) and b) (3) (see Fig. 5). Data are fitted with the exponential law (6) for early times, and with the algebraic law (11) for late times.

if h_0 is the radius of the filament at that point when the respective droplets start growing. Using Eq. (7), we have converted the observed growth rates into an effective viscosity, to be compared to the extensional viscosity reported in Table II.

The temporal behavior of beads of type (2) and (3) (see Fig. 5) is more complicated, as it shows two different growth regimes, see Fig. 8. At first their growth is exponential, as described by Eq. (6), but with growth rates ω smaller than type (1) beads. After a period of 5 to 7 ms, the time dependence of the amplitude changes from convex to concave (Fig. 8). In this second stage, the amplitude increases much faster, as a result of *pumping* by the connecting filament, as we will argue now. The radius of the filament is much smaller than the radius of the droplet and thus the Laplace pressure is higher. Volume conservation describes how the volume of the drop V_S increases as that of the volume of the filament V_C decreases,

$$\frac{dV_S}{dt} = -\frac{dV_C}{dt}. \tag{8}$$

We model the drop as a sphere of radius r_S, giving $V_S = \frac{4}{3}\pi r_S^3$, while the filament is described as a cylinder of length l and radius h_0: $V_C = \pi h_0^2 l$. For the regime where the polymer chains have become fully stretched, the filament radius is expected to follow a linear law,[20]

$$h_0(t) = \alpha \frac{\gamma}{\eta_{eff}} (t_0 - t). \tag{9}$$

Here t_0 is the extrapolated time of break-up, and the prefactor $\alpha = 0.07$ is a numerical constant appropriate for the similarity solution describing viscously dominated break-up. The data are not sufficiently accurate to identify the crossover from viscous to viscous-inertial pinching,[14] so we only use a single linear law. Note that in actual fact break-up does not occur, but the filament is ultimately stabilized as a solid thread is formed, as described in Sec. VI.

Inserting Eq. (9) into Eq. (8) and calculating the time derivative, one gets

$$\frac{dV_S}{dt} = 2\pi l B^2 (t_0 - t), \tag{10}$$

with $B = \alpha\gamma/\eta_{eff}$. Integrating and solving for V_S one finds that the amplitude $a(t) = r_S(t) - r_C$ is

$$a_p(t) = \left[\Gamma\left(t_0 t - \frac{1}{2}t^2\right) + r_C^3\right]^{1/3} - r_C, \tag{11}$$

where we have put $\Gamma = 3lB^2/2 = 3l(\alpha\gamma/\eta_{eff})^2/2$, and r_C is the radius of the cylindrical filament. Figure 8 shows that this power law well describes the data in the second growing regime. The only fitting parameter is Γ from which we get $l \approx 800\,\mu$m which seems a reasonable estimate for the length from which the droplet is pumped.

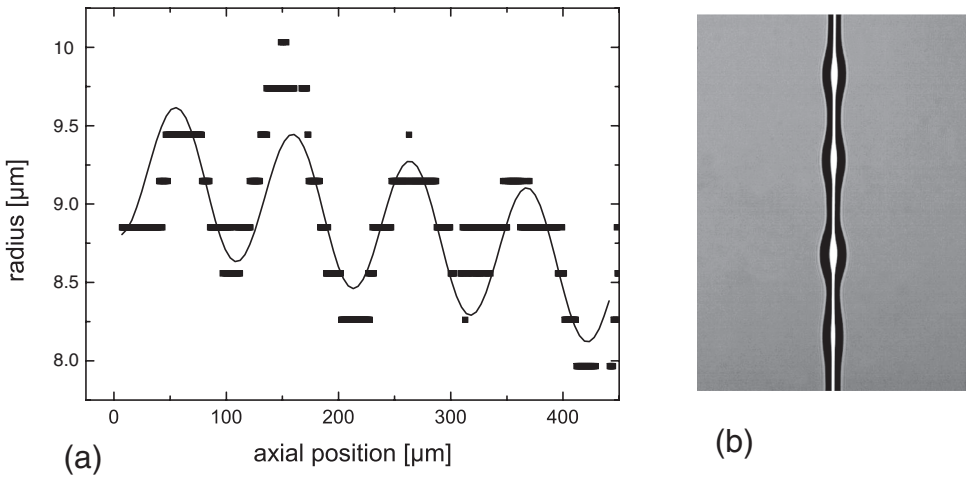

FIG. 9. Radial profile of several droplets growing collectively, with a sinusoidal fit according to Eq. (12).

B. Periodic perturbations

The fourth type of linear instability is the growth of sinusoidal perturbations on the filament (type (4), see Fig. 5). As illustrated in Fig. 9, the deformation of the interface is fitted by

$$h(z,t) = h_0(t) + s(t)z + a(t)\sin\left(2\pi\frac{z - z_0(t)}{\lambda(t)}\right), \tag{12}$$

$r_0(t)$ is the radius of the unperturbed cylindrical filament. The linear piece $s(t)z$ accounts for the slightly conical shape of the filament. The wavelength $\lambda(t)$ is allowed to change in time, and $a(t)$ is the amplitude of the perturbation. Figure 9 shows how Eq. (12) is fitted to a perturbation at the limit of the pixel resolution of our system. In Ref. 14, we describe how this method can be used to achieve spatial resolution of 80 nm.

Figure 10 shows the growth of the amplitude of the sinusoidal pattern. We observe exponential behavior until smaller beads start to grow between the primary beads, making the dynamics nonlinear. This phenomenon will be discussed in Sec. V. Lacking a complete stability theory for this highly

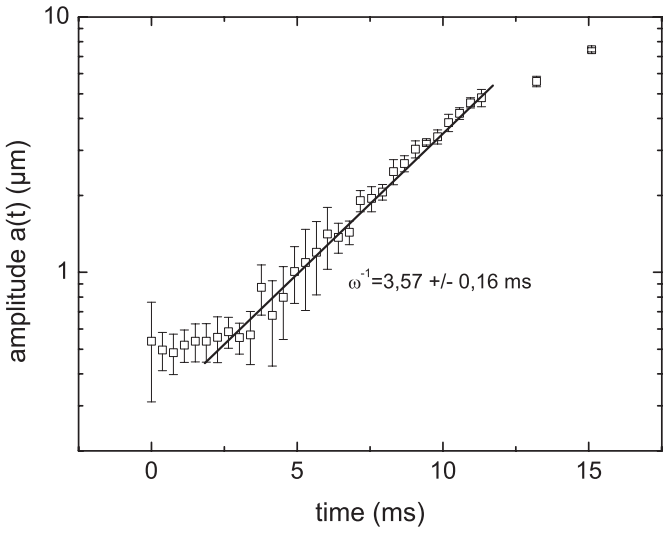

FIG. 10. Temporal evolution of the amplitude of coherent beads (4), using Eqs. (6) and (12).

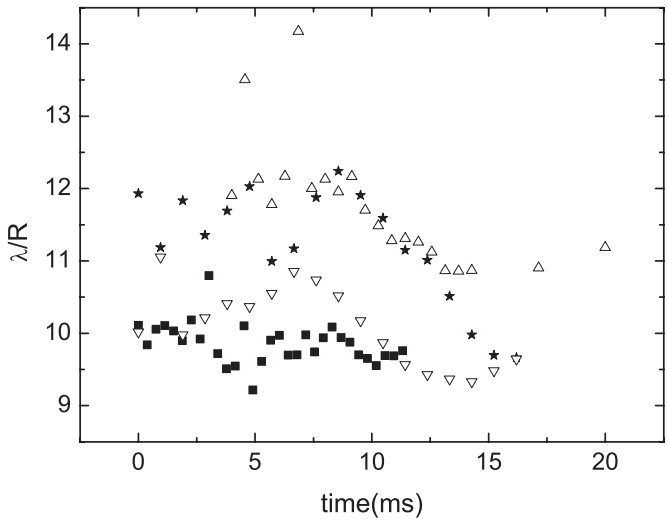

FIG. 11. The reduced wavelength λ/h_0 for the perturbation (12) for four different experimental runs.

stretched state, we once more use Eq. (7) to deduce an effective elongational viscosity η_{eff}; the values are listed in Table II.

As seen in Fig. 11, the wavelength remains constant to a good approximation over the growth of the sinusoidal perturbation. This is consistent with the assumption of a linear instability. There is some scatter in the numerical value, but λ/h_0 is generally between 9 and 12, just above the value generally accepted for the Rayleigh–Plateau theory of *inviscid* pinch-off.[2] This is surprising, since the effective viscosity has risen to much higher values. Indeed, once we have determined η_{eff}, we can estimate the wavelength of the most unstable perturbation according to Ref. 2,

$$\frac{\lambda}{h_0} = 2\pi\sqrt{2 + \eta_{eff}\sqrt{\frac{18}{\rho h_0 \gamma}}}. \tag{13}$$

This yields typical values of $\lambda/h_0 \approx 175$, much larger than what is observed in experiments.

A possible explanation is that a solid core as formed at the center of the thread, a scenario that will be explored further in Sec. VI. A linear stability analysis of a Newtonian fluid thread with a cylindrical solid core has been investigated in Ref. 27. In the absence of inertia, the effect of the solid core is to shift the most unstable wavelength to much smaller values, even if the radius of the solid core is smaller than that of the thread by orders of magnitude. If we estimate the radius of the solid core as $h_c \approx 50$ nm, as suggested by Fig. 15 below, and the radius of the thread as $h_0 \approx 10\,\mu$m, we find a ratio of $h_c/h_0 \approx 5 \times 10^{-3}$. Then in the limit large viscosities (inertial effects are negligible), Fig. 2 of Ref. 27 predicts a wavelength $\lambda/h_0 \approx 4\pi$, which is consistent with Fig. 11.

Table II summarizes estimates for the effective viscosity η_{eff}, as calculated based on the various instability mechanisms described above. It is clear that there are considerable discrepancies between the different results. First, using the estimates based on the various types of linear instabilities, values vary between 1 Pas and 12 Pas. These differences might be caused by the different flow histories: the base solution on which a bead at the upper end, exhibiting an inward bulge, is quite different from that at the lower end. Clearly, there is an influence of gravitational sagging. The effective viscosity deduced from the final linear thinning behavior via Eq. (9) yields $\eta_{eff} \approx 8$ Pas, which is roughly consistent.

However, strong disagreement exists between the effective viscosities estimated from instabilities, and that calculated from exponential thinning, as observed earlier.[14] According to the standard picture, the extensional viscosity resulting from stretching should set the effective viscosity scale.[20] Once polymers have become fully stretched, the viscosity can no longer increase, and the fluid once more has Newtonian behavior, but with a much elevated viscosity. However, according to Table II,

the extensional viscosity based on polymer stretching is about two orders of magnitude greater. In other words, the linear instabilities evolve on a time scale that is much too fast. We do not yet have a conclusive explanation for these discrepancies. However, in Sec. VI, we will argue that a phase separation between fluid and solid components takes place. This would rationalize that the fluid component contains fewer polymers than in a uniformly mixed state, and thus possesses a lower viscosity than predicted by the standard model.

V. THE NEXT GENERATIONS

The data in this chapter are taken using the PEO_{1k-w} and the PEO_{2k-w} solution. After the formation of a periodic array of beads, further generations of beads start to grow (Fig. 12). First the form of the periodic deformation becomes nonlinear and a pattern of beads of equal size on a straight filament is formed. In between these filaments, a new generation of smaller droplets starts to grow. The data did not allow to extract any growth rates for these droplets, but eventually the size of the second generation beads also saturates,[12] and a third generation of beads is formed between the first and the second one. We were able to resolve separate beads up to the fourth generation, but we found that only the first three generations of secondary beads appeared in a well defined chronological order.

As described in the Introduction, the formation of secondary beads on a polymeric filament has been investigated theoretically in Ref. 21. In particular, Chang *et al.*[21] propose a *recursive* mechanism for the radius of the consecutive filaments of number n of the form

$$h_n/h_0 = \sqrt{2}(h_{n-1}/h_0)^{3/2}. \tag{14}$$

However, this power law could not be reproduced by Refs. 12 and 13, but a power law exponent closer to $m = 2$ was found, instead of $m = 3/2$.

Instead of the thread radii, we decided to measure the distribution of the final, stationary sizes of beads of different generations, which can be measured with higher resolution than the thread diameters, owing to their greater size. If the process of bead formation is iterative, the final bead sizes are also expected to be self-similar, and their size ratios to correspond to that of the threads. We have however not tested for this latter fact. More than 130 droplets from different experimental runs were measured, and the results summarized in a histogram (Fig. 13). The histogram clearly shows preferred sizes for the different droplet generations.

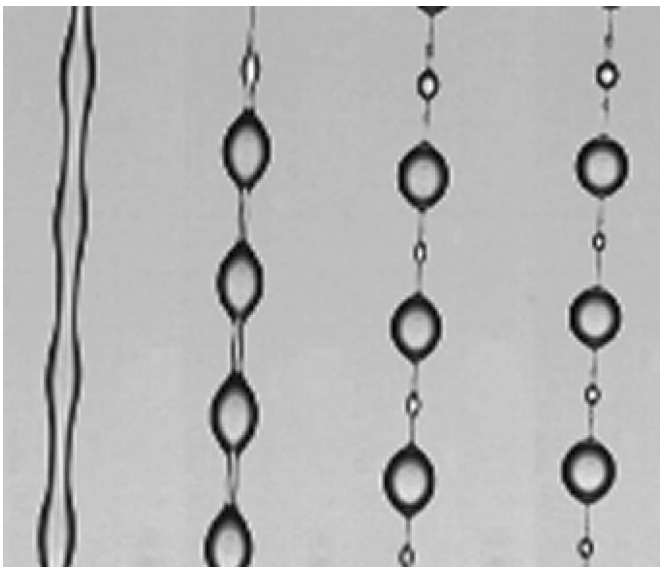

FIG. 12. Growth of secondary droplets on a regular array of primary beads. Three generations of beads are visible.

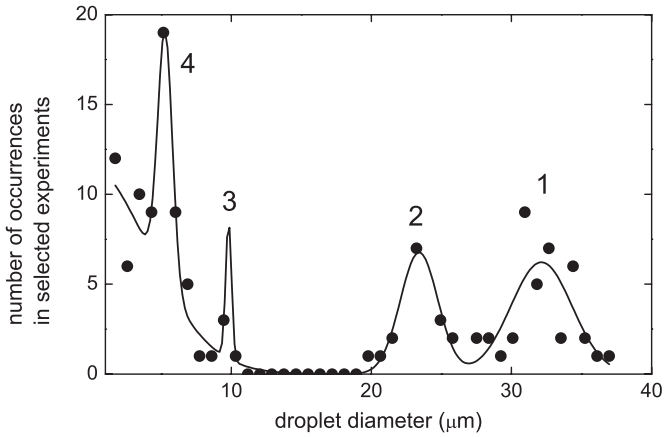

FIG. 13. Histogram of the distribution of the final diameters of the droplets that are formed on the filament (cf. Fig. 12) of a PEO_{1k-w} solution in a CaBER experiment. More than 130 droplets have been evaluated. The lines are Gaussian fits with a background offset to determine the mean diameters.

From the peak values, mean diameters of $D = 32.1$, 23.4, 9.8, and 5.3 ± 0.1 μm for the first four generations of droplets can be estimated. However, the distribution shows a significant background signal for droplet sizes below 10 μm and it was not possible to distinguish more different sizes. A possible iterative character of the process of secondary bead formation is investigated in Fig. 14. We have plotted the size of beads of generation $n + 1$ as function of the size of the previous generation in a double logarithmic plot for a similar solution as in Ref. 12. Toward larger bead sizes there is some indication of self-similarity, and an exponent 3/2 can be fitted. This is consistent with the scaling found by Ref. 12, if indeed the scaling of beads and threads correspond.

VI. FORMATION OF NANO FIBERS

In Ref. 14, it was shown that the final long lasting filament of a PEO_{2k-w} solution with the remaining droplets could be carefully transferred on a metallic carrier and placed in a scanning electron microscope, as seen in Fig. 15. The nano fiber shown here has a thickness of 80 nm and it is reasonable to assume that the polymers are fully elongated and partially crystallized.

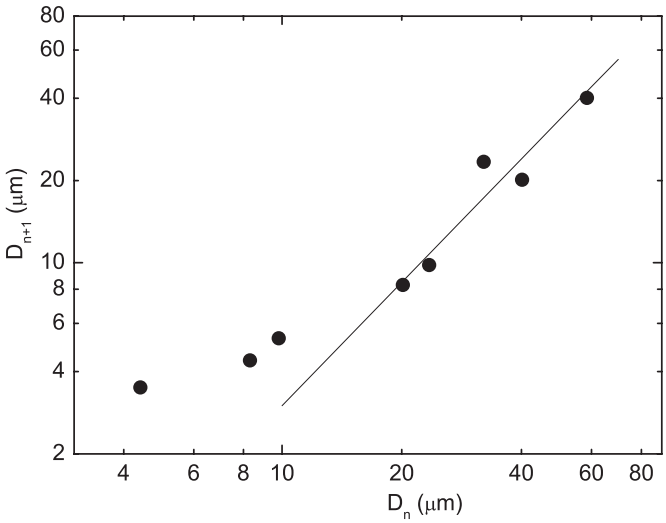

FIG. 14. The droplet diameter D_{n+1} of a PEO_{2k-w} solution plotted as function of the preceeding generation D_n, in a double logarithmic plot. The line has a slope of 3/2.

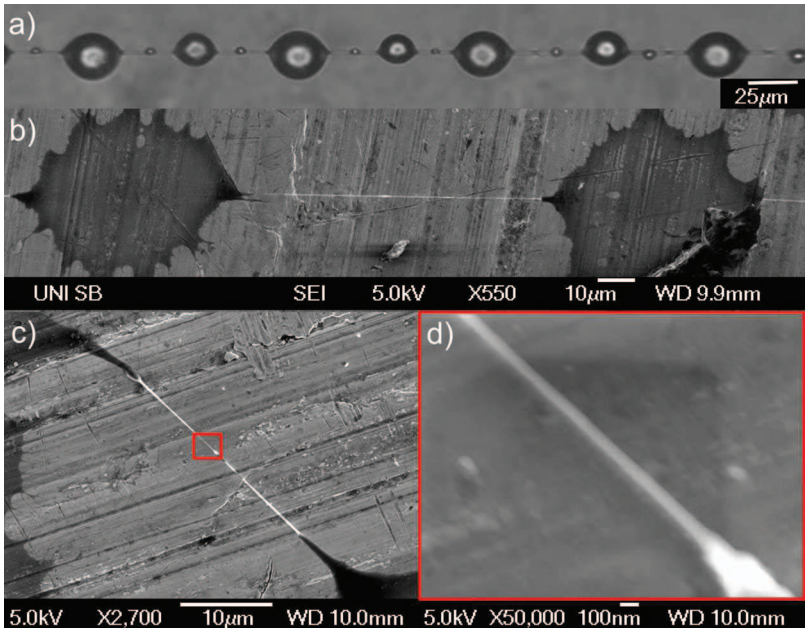

FIG. 15. (Color online) (a) Shadowgraph image of a typical beads-on-a-string pattern (taken from Ref. 14). The droplets are arranged off-axis relatively to the thread. (b) Scanning electron microscopy image of two beads, connected by a thread (intermediate resolution). The structure was caught and dried upon the substrate. (c) Another example of the structure. (d)A close up of (c) at high magnification.

A. Optical *in situ* indications

The scanning electron microscopy (SEM) images in Fig. 15 show the existence of a solid nano fiber, but we would like to present its first indications which we found on our shadowgraph images (Figs. 16 and 17). The fiber itself is too thin to be resolved in the images, but often a pattern as shown in Fig. 15(a) was formed. What is remarkable is that most beads are off-center with respect to the filament. Comparison with the problem of fluid droplets on a fiber[28] shows that there must be a *finite* contact angle between the droplets and the filament for such a symmetry breaking to occur. In other words, the thin filament must have formed a (solid) phase different from that of the droplets.[29]

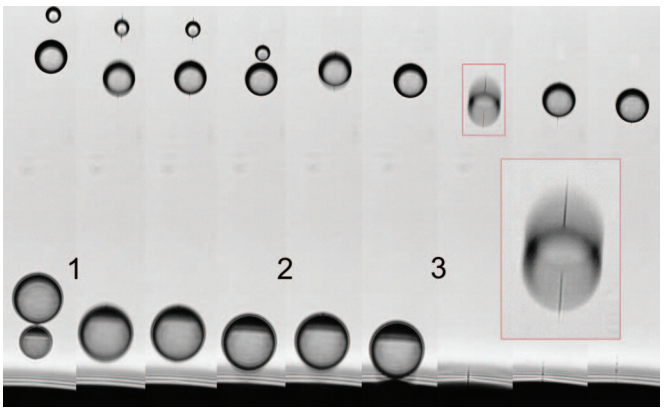

FIG. 16. (Color online) The coalescence of droplets at later stages of the blistering process reveals the existence of a nano fiber. The numbers 1–3 indicate three different coalescence events at time t= 325 ms (1), 333 ms (2), and 338 ms (3). The merging of droplets leads to stress that is released in an oscillatory manner. The droplets move up and down along the fiber that gets wetted and becomes darker in the images (see the magnification at the lower right hand site).

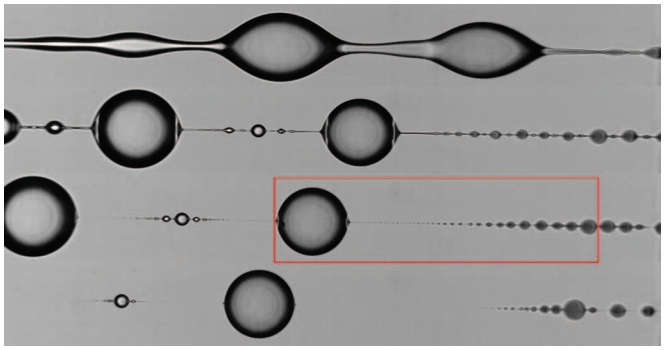

FIG. 17. (Color online) The late stages of the blistering process of an aqueous solution of a PEO_{1k-w} solution. The first image is at $t = 250$ ms after the formation of the cylindrical filament. Subsequent images are taken every 30 ms. The images show that a thin fiber with the small beads is drawn out of the large droplet. The online movie shows a high speed video of a 200 ms sequence at a 40 times slower rate (enhanced online) [URL: http://dx.doi.org/10.1063/1.3684750.1].

A second indirect indication was observed when the droplets on the filament did merge. This led to an abrupt increase in stress which was released in an oscillatory manner. The droplets then moved up and down, or rather slide up and down over the thin filament which are wetted as one can see in Fig. 16.

Another estimate of the size of the remaining nano fiber could be deduced from Fig. 17 (see online movie available at http://dx.doi.org/10.1063/1.3684750.1 for the image sequence). Apparently, the thin filament that was connected to the larger bead was not a simple polymeric solution anymore, but showed properties of a purely elastic fiber. This fiber is under large tension and it pulled out more material from the larger droplet, just as in the case of fiber spinning.[30,31] The filament becomes longer by pulling out material and in all experiments it was observed that if this happened it was always the largest droplet from the cascade of droplets from which the material was drawn. We used this pattern to estimate the size distribution of the smaller droplets (Fig. 18). The size of the larger droplets could be measured directly and the sizes of the smallest beads are arranged linearly. We do not have any explanation for this, but we used this linear regime to extrapolate the sizes of the smallest droplet of which the positions could be detected optically, but not the sizes. This approach might be very simple, but it should be taken as an estimate only. We found that the smallest droplets are probably only 300 nm in size and the surrounding fiber has to be significantly thinner. Otherwise their positions deduced from their diffraction patterns could not have been separated from the overall diffraction pattern of the connecting cylindrical filament.

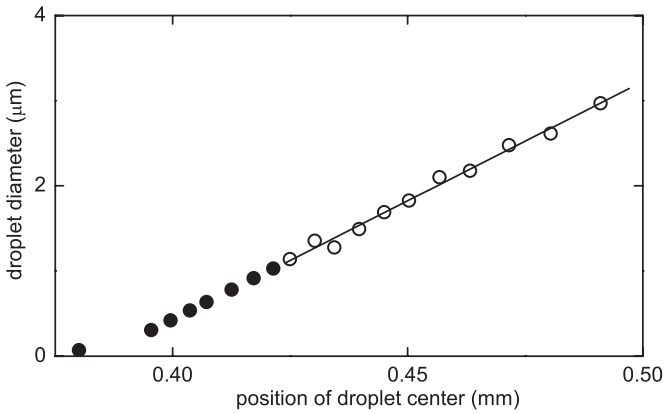

FIG. 18. Sizes of the droplets of different generations. Open symbols indicate droplet sizes that could be measured directly and full symbols indicate droplets that were to small for a size estimation, but a position determination was still possible (cf. Fig. 17). The line is ar linear fit.

B. The effect of evaporation

In order to clarify whether evaporation was responsible for the formation of the solid fiber, we performed experiments in a liquid–liquid system. A small glass cell was built and silanized to prevent wetting of the glass by the aqueous phase. The cell was filled with a low viscous silicone oil (Dow Corning 200, η= 5 mPas) and we added a fluorescent dye (Rhodamin 6 G) to our PEO_{2k-w} solution. The polymeric sample was pumped slowly through a nozzle (diameter d = 2 mm) into the surrounding silicone oil. The experiment was illuminated with a green laser (Quantrum, power = 150 mW) and a dichroic filter that passed the fluorescence signal was placed between the microscope lens and the camera. Droplets detaching from the nozzle fell to the bottom plate that was 1 cm apart. The formation of the cylindrical thread, the characteristic time constant and the blistering process did not differ qualitatively from our observations at the free surface. Most importantly, at the position where the filament should be, there was always a very thin line to see that remained for many seconds until bleaching of the dye occurred. The signal was too weak to allow for a quantitative evaluation, but was sufficient to be observable on the screen. Thus, we can exclude that evaporation which plays a significant role in the phenomenon discussed above, and the phase separation is rather flow induced.[32]

C. Other polymer solutions

PEO is known to have a limited solubility in water and the solutions described above might have been close to the cloud point. Four more solutions (see Table I) were tested to verify the generality of our observation of a solid nano fiber. Furthermore, we chose two systems with very low vapor pressure, again to verify that evaporation does not play a key role in our experiments.

The blistering pattern and the formation of the nano fiber could be reproduced for all solutions. First a c = 2000 ppm PEO solution in xylol (PEO_{2k-x}) was investigated (Fig. 19). Some differences in the substructures of the dried remains of the droplets compared to the PEO in water solutions are apparent, but besides this the SEM images look very similar. The solutions of polystyrene in dimethylformamide represent a completely different class of polymer-solvent systems. The SEM images of the dried remains look qualitatively different and the nano fiber is considerably thicker. A transition from a smooth and well ordered fiber to a less ordered state is apparent (Fig. 20), the former being the remainder of the thread, the latter that of the droplet.

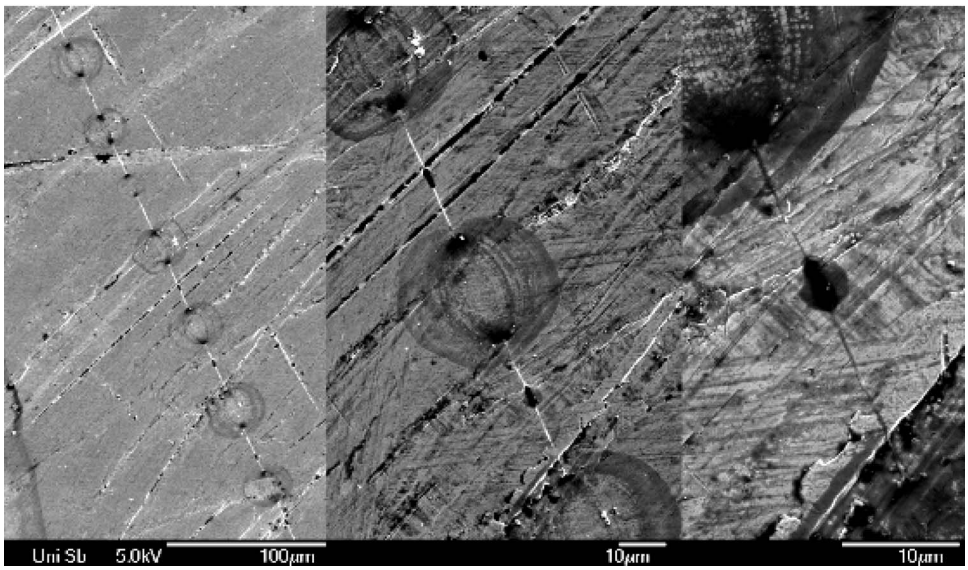

FIG. 19. SEM images of the dried remains of a polymer solution, showing the blistering pattern on a nano fiber for 2000 ppm PEO in xylol. The images are successive magnifications.

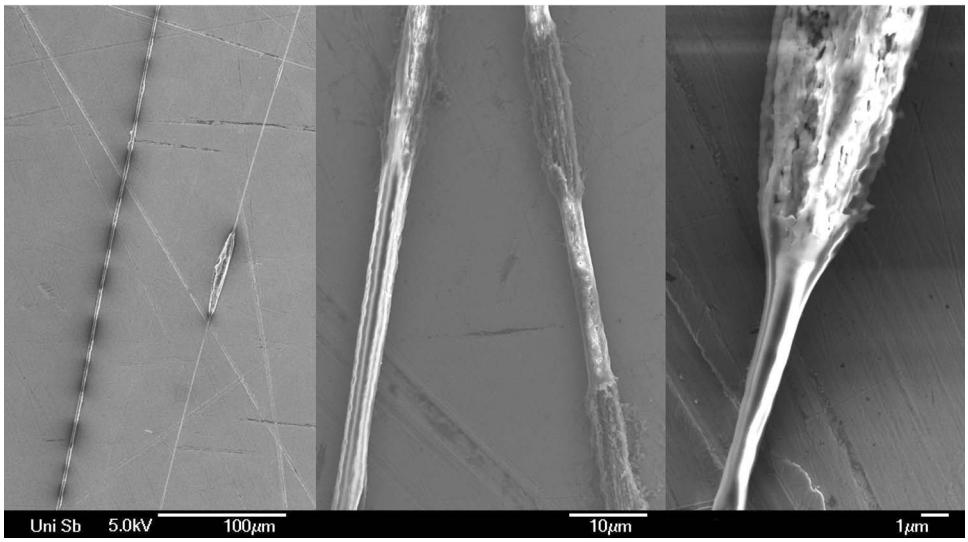

FIG. 20. Images of the dried remains of a solution of polystyrene in dimethylformamide, which show a blistering pattern. The images are different magnifications of different samples.

For the experiments with poly(acrylamid-co-acrylic acid) (PAAA) the solvent was a sugar water solution, see Fig. 21. These experiments are also very illustrative because the sugar in the dried filament stabilizes the blistering pattern enough to allow the formation of very stable structures of a length of many centimeters that can easily be carried around. Note that it is also possible to draw thin sugar fibers without the help of any polymers as it is used for cotton candy.

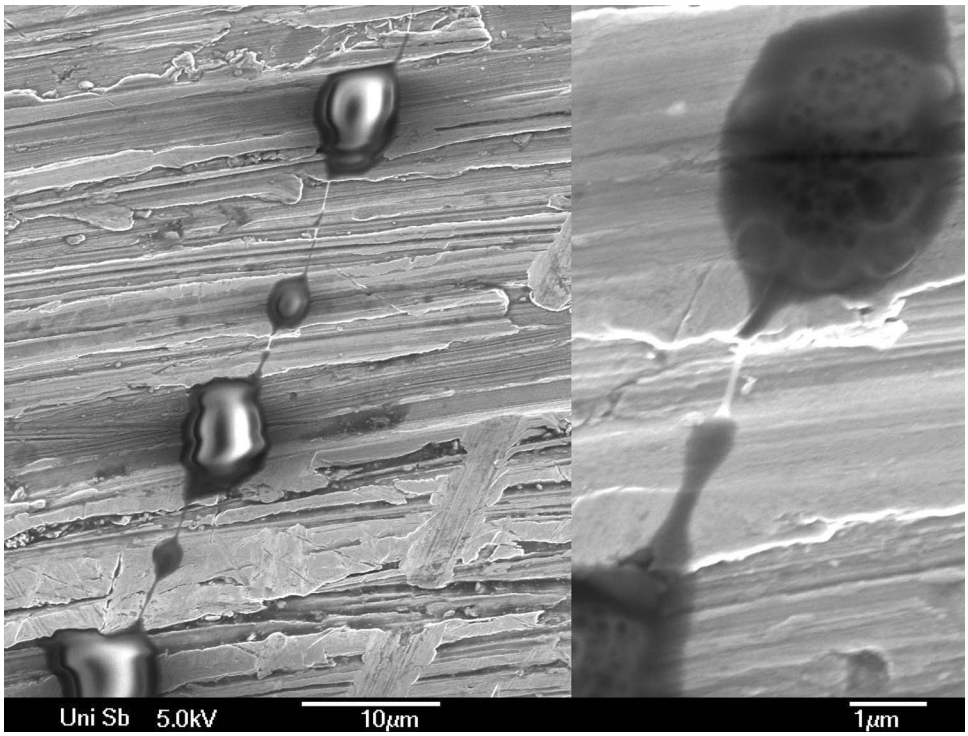

FIG. 21. Blistering pattern of a solution of PAAA in sugar water. The right image is a magnification of the left image.

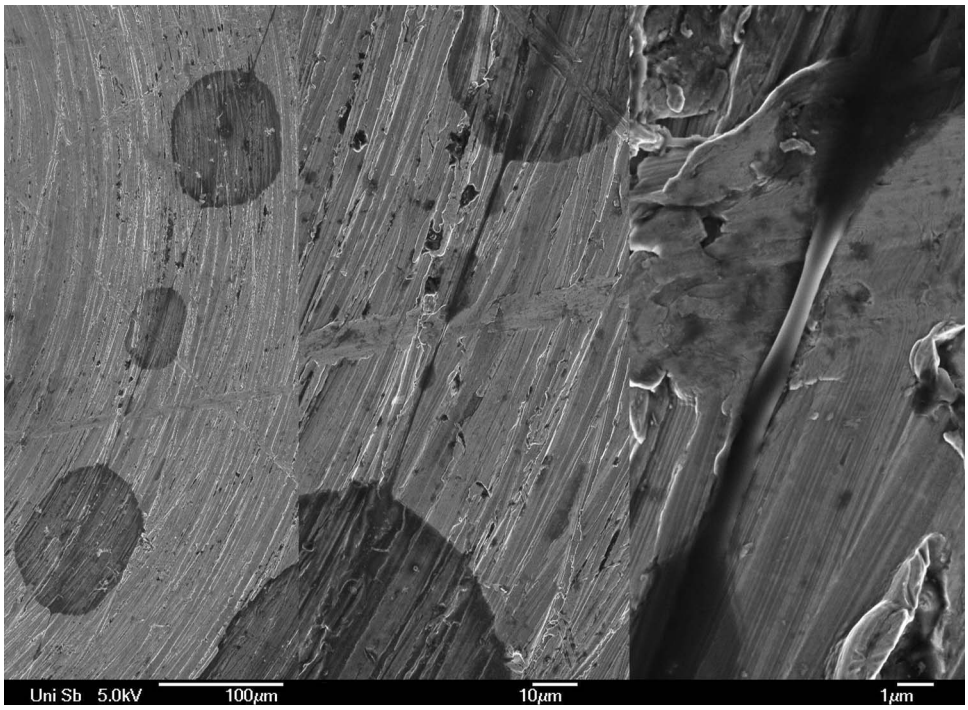

FIG. 22. SEM images of a blistering pattern of a sample of saliva. The consecutive images are different magnifications.

Finally, we performed experiments with saliva from one healthy donor and we could reproduce the SEM images for droplets of saliva as well (Fig. 22). In saliva, glycoproteins such as mucin are suspected to be responsible for the polymeric effect.

VII. CONCLUSIONS

In conclusion, we have presented a study on the final stages of the capillary break-up of semi-dilute polymer solutions. For some of our measurements we could evaluate the light intensity distribution of the Fresnel diffraction around the filament. This allowed us to improve the spatial resolution down to an precision of 30 nm. We found that the droplets that formed along the filament at the final stages of the thinning process could be separated into four classes: droplets at the lower and the upper end of the filament, droplets growing in the interior of the filament, and droplets growing coherently. The growth of droplets is always exponential at first, demonstrating a linear instability of the polymeric filament.

We have presented plenty of evidence that the formation of small beads investigated by us results from the instability of a highly stretched state, a process we termed "blistering". The alternative "beads-on-a-string" process[15,18] relies on the inertia imparted on the system from the primary instability. As a result, the solvent viscosity is an important parameter for the formation of the "beads-on-a-string" structure, while it is unimportant for the bead formation investigated in the present paper. To summarize, we have found that bead formation:

(i) proceeds from a uniform filament, which is thinning exponentially,
(ii) is independent of solvent viscosity,
(iii) only starts when the polymers have reached almost full stretch, as indicated by the extensional viscosity having reached saturation,
(iv) is associated with a crossover from exponential to linear in the thinning rate,
(v) is associated with exponential growth relative to the uniform state.

Subsequently, we investigated the nonlinear stages of the instability. Some of the droplets are pumped by the surrounding filament, leading to power-law growth. Eventually, the size of all droplets reaches a plateau value. Owing to interaction between beads or droplets, a hierarchy of bead sizes is produced, showing a limited degree of self-similarity. Finally, we described the formation of a solid nano fiber out of the liquid-polymer solution. The formation of the solid fiber is the result of a flow induced phase separation, as evaporation does not play a significant role. The formation of the nano fiber has been confirmed using scanning electron microscopy for a variety of different polymer-solvent systems.

ACKNOWLEDGMENTS

This work was supported by the DFG-Project WA 1336 and Thermo Haake.

[1] J. Eggers, "Universal pinching of 3D axisymmetric free-surface flow," Phys. Rev. Lett. **71**, 3458 (1993).
[2] J. Eggers and E. Villermaux, "Physics of liquid jets," Rep. Prog. Phys. **71**, 036601 (2008).
[3] C. Wagner, Y. Amarouchene, D. Bonn, and J. Eggers, "Droplet detachment and satellite bead formation in visco-elastic fluids," Phys. Rev. Lett. **95**, 164504 (2005).
[4] Y. Amarouchene, D. Bonn, J. Meunier, and H. Kellay, "Inhibition of the finite-time singularity during droplet fission of a polymeric fluid," Phys. Rev. Lett. **86**, 3558 (2001).
[5] M. Goldin, J. Yerushalmi, R. Pfeffer, and R. Shinnar, "Breakup of a laminar capillary jet of a viscoelastic fluid," J. Fluid Mech. **38**, 689 (1969).
[6] A. V. Bazilevskii, S. I. Voronkov, V. M. Entov, and A. N. Rozhkov, "Orientational effects in the decomposition of streams and strands of diluted polymer solutions," Sov. Phys. Dokl. **26**, 333 (1981).
[7] V. M. Entov and A. L. Yarin, "Influence of elastic stresses on the capillary breakup of dilute polymer solutions," Fluid Dyn. **19**, 21 (1984).
[8] M. Stelter, G. Brenn, A. L. Yarin, and P. Singh, "Validation and application of a novel elongational device for polymer solutions," J. Rheol. **44**, 595 (2000).
[9] S. L. Anna and G. H. McKinley, "Elasto-capillary thinning and breakup of model elastic liquids," J. Rheol. **45**, 115 (2001).
[10] C. Clasen, J. Eggers, M. A. Fontelos, J. Li, and G. H. McKinley, "The beads-on-string structure of viscoelastic jets," J. Fluid Mech. **556**, 283 (2006).
[11] S. Middleman, "Stability of a viscoelastic jet," Chem. Eng. Sci. **20**, 1037 (1965).
[12] M. S. N. Oliveira and G. H. McKinley, "Iterated stretching and multiple beads-on-a-string phenomena in dilute solutions of high extensible flexible polymers," Phys. Fluids **17**, 071704 (2005).
[13] M. S. N. Oliveira, R. Yeh, and G. H. McKinley, "Iterated stretching, extensional rheology and formation of beads-on-a-string structures in polymer solutions," J. Non-Newtonian Fluid Mech. **137**, 137 (2006).
[14] R. Sattler, C. Wagner, and J. Eggers, "Blistering pattern and formation of nanofibers in capillary thinning of polymer solutions," Phys. Rev. Lett. **100**, 164502 (2008).
[15] J. Li and M. A. Fontelos, "Drop dynamics on the beads-on-string structure of viscoelastic jets: A numerical study," Phys. Fluids **15**, 922 (2003).
[16] V. Tirtaatmadja, G. H. McKinley, and J. J. Cooper-White, "Drop formation and breakup of low viscosity elastic fluids: Effects of molecular weight and concentration," Phys. Fluids **18**, 043101 (2006).
[17] J. Etienne, E. J. Hinch, and J. Li, "A Lagrangian-Eulerian approach for the numerical simulation of free-surface flow of a viscoelastic material," J. Non-Newtonian Fluid Mech. **136**, 157 (2006).
[18] P. P. Bhat, S. Appathurai, M. T. Harris, M. Pasquali, and G. H. McKinley, "Formation of beads-on-a-string structures during break-up of viscoelastic laments," Nat. Phys. **6**, 625 (2010).
[19] R. B. Bird, R. C. Armstrong, and O. Hassager, *Dynamics of Polymeric Liquids. Volume I: Fluid Mechanics* (Wiley, New York, 1987); *Volume II: Kinetic Theory* (Wiley, New York, 1987).
[20] M. A. Fontelos and J. Li, "On the evolution and rupture of filaments in Giesekus and FENE models," J. Non-Newtonian Fluid Mech. **118**, 1 (2004).
[21] H.-C. Chang, E. A. Demekhin, and E. Kalaidin, "Iterated stretching of viscoelastic jets," Phys. Fluids **11**, 1717 (1999).
[22] R. Sattler, Ph.D. dissertation, Universität des Saarlandes, 2009.
[23] E. Miller, C. Clasen, and J. P. Rothstein, "The effect of step-stretch parameters on capillary breakup extensional rheology (caber) measurements," Rheol. Acta **48**, 625 (2009).
[24] L. Campo-Deaño and C. Clasen, "The slow retraction method (SRM) for the determination of ultra-short relaxation times in capillary breakup extensional rheometry experiments," J. Non-Newtonian Fluid Mech. **165**, 1688 (2010).
[25] A. Zell, S. Gier, S. Rafay, and C. Wagner, "Is there a relation between the relaxation time measured in caber experiments and the first normal stress coefficient?," J. Non-Newtonian Fluid Mech. **165**, 1265–1274 (2010).
[26] J. P. Plog, W. M. Kulicke, and C. Clasen, "Influence of the molar mass distribution on the elongational behaviour of polymer solutions in capillary breakup," Appl. Rheol. **15**, 28 (2005).
[27] S. L. Goren, "The instability of an annular thread of fluid," J. Fluid Mech. **12**(2), 309 (1962).
[28] B. J. Carroll, "Equilibrium conformations of liquid drops on thin cylinders under forces of capillarity. a theory for the roll-up process," Langmuir **2**, 248 (1986).
[29] D. F. James and J. H. Saringer, "Extensional flow of dilute polymer solutions," J. Fluid Mech. **97**, 655 (1980).

[30] J. Smook, A. J. Pennings, and D. Quéré, "Elastic flow instabilities and shish-kebab formation during gel-spinning of ultra-high molecular weight polyethylene," J. Mater. Sci. **19**, 31 (1984).
[31] P. J. Barham and D. Quéré, "Strong polymer fibres," Phys. Technol. **17**, 167 (1986).
[32] T. Kume, T. Hashimoto, T. Takahashi, and G. G. Fuller, "Rheo-optical studies of shear-induced structures in semidilute polystyrene solutions," Macromolecules **30**, 7232 (1997).